THE ASTROPHYSICAL JOURNAL, 456:L71–L74, 1996 January 10

MSAM1-94: REPEATED MEASUREMENT OF MEDIUM-SCALE ANISOTROPY IN THE COSMIC MICROWAVE BACKGROUND RADIATION

E. S. CHENG,[1] D. A. COTTINGHAM,[2] D. J. FIXSEN,[3] C. A. INMAN,[4] M. S. KOWITT,[1] S. S. MEYER,[4]
L. A. PAGE,[5] J. L. PUCHALLA,[4] J. E. RUHL,[4] AND R. F. SILVERBERG[1]
Received 1995 August 25; accepted 1995 October 25

ABSTRACT

The second flight of the Medium-Scale Anisotropy Measurement (MSAM1-94) observed the same field as the first flight (MSAM1-92) to confirm our earlier measurement of cosmic microwave background radiation (CMBR) anisotropy. This instrument chops a 30′ beam in a three-position pattern with a throw of ±40′ and simultaneously measures single- and double-differenced sky signals. We observe in four spectral channels centered at 5.6, 9.0, 16.5, and 22.5 cm^{-1}, providing sensitivity to the peak of the CMBR and to thermal emission from interstellar dust. The dust component correlates well with the *IRAS* 100 μm map. The CMBR observations in our double-difference channel correlate well with the earlier observations, but the single-difference channel shows some discrepancies. We obtain a detection of fluctuations in the MSAM1-94 data set that match CMBR in our spectral bands of $\Delta T/T = 1.9^{+1.3}_{-0.7} \times 10^{-5}$ (90% confidence interval, including calibration uncertainty) for total rms Gaussian fluctuations with correlation angle 0.°3, using the double-difference demodulation.

Subject headings: balloons — cosmic microwave background — cosmology: observations

1. INTRODUCTION

Observations of anisotropy in the cosmic microwave background radiation (CMBR) yield valuable clues about the formation of large-scale structure in the early universe. A particularly interesting angular scale for observing CMBR anisotropy is near 0.°5, where the first "Doppler peak" (or adiabatic peak) enhancement of the fluctuation power spectrum is expected to be observable (White, Scott, & Silk 1994). The Medium-Scale Anisotropy Measurement (MSAM) is an experiment designed to measure CMBR anisotropy at this angular scale. This paper reports the initial results from the second flight of this experiment.

A number of detections of anisotropy at angular scales near 0.°5 have been reported recently. Observations by ARGO (de Bernardis et al. 1994), the Python experiment (Dragovan et al. 1994), the fourth flight of the MAX experiment (Devlin et al. 1994; Clapp et al. 1994), SK94 (Netterfield et al. 1995), and SP94 (Gundersen et al. 1995) all report detections of anisotropy near this angular scale.

Quantifying CMBR anisotropy at the level of these detections is an extremely challenging observational task (Wilkinson 1995). Many potential systematic errors cannot be unequivocally ruled out at the necessary levels, with the result that no single observation can prudently be accepted without an independent confirmation. The results in this Letter are our attempt to confirm the results of our previous work. By observing the same region of the sky with a second balloon flight, we demonstrate the repeatability of our measurements in the presence of potential atmospheric noise and contamination from earthshine.

We have reported earlier (Cheng et al. 1994, hereafter Paper I) our observations of anisotropy of the CMBR from the first flight of MSAM in 1992. Our results from those observations were (1) a positive detection of anisotropy, with the caveat that we could not rule out foreground contamination by bremsstrahlung, and (2) the identification of two particular bright spots that were consistent with being unresolved sources. This paper reports our first results from the 1994 flight of MSAM, which observed an overlapping field.

2. INSTRUMENT DESCRIPTION

This instrument has been briefly described in Paper I; we give only an overview here. It has four spectral bands at 5.6, 9.0, 16.5, and 22.5 cm^{-1}, giving sensitivity to CMBR and Galactic dust. The off-axis Cassegrain telescope forms a 30′ beam on the sky. The chopping secondary mirror moves this beam in a step motion 40′ left and right of center. The beam moves center, left, center, right with a period of 0.5 s. The detectors are sampled at 32 Hz synchronously with the chop.

The telescope is mounted on a balloon-borne platform stabilized with a gyroscope. Periodically during flight we manually null the position error and gyroscope drift rate by using a CCD star camera as an absolute pointing reference. The telescope is shielded with aluminized panels, so that the Dewar feed horn, the secondary, and most of the primary have no direct view of the Earth.

The gondola superstructure changed between the 1992 and 1994 flights. The previous superstructure as viewed from the telescope had a substantial cross section of reflective material; in spite of our efforts to shield it, we were concerned about the telescope being illuminated by reflected earthshine. The new design is a cable suspension with considerably lower cross section above the telescope. Ground measurements indicate that rejection of signals from sources near the horizon is better than 70 dB unchopped and 85 dB chopped in our longest

[1] Laboratory for Astronomy and Solar Physics, NASA/Goddard Space Flight Center, Code 685.0, Greenbelt, MD 20771.
[2] Global Science and Technology, Inc., Laboratory for Astronomy and Solar Physics, NASA/GSFC Code 685.0, Greenbelt, MD 20771.
[3] Applied Research Corporation, Laboratory for Astronomy and Solar Physics, NASA/GSFC Code 685.3, Greenbelt, MD 20771.
[4] Enrico Fermi Institute, University of Chicago, 5640 South Ellis Avenue, Chicago, IL 60637.
[5] Physics Department, Princeton University, Princeton, NJ 08544.

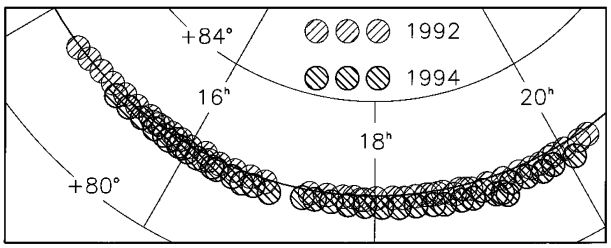

FIG. 1.—Hatched circles show the sky coverage for the 1992 and 1994 flights as derived from the sky binning procedure. The beam size and chop spacing are indicated in the legend on the top of the plot. The region shown covers R.A. $14^h.0$–$20^h.5$ and declination +80°–+84°. The average declination difference between the two flights is 10′.

wavelength channel. This alone, however, is not a sufficient basis for us to argue that our results are uncontaminated by Earth emission; as we discuss below, this is demonstrated by the consistency of observations taken at different times.

3. OBSERVATIONS

The package was launched from Palestine, Texas, at 00:59 UT on 1994 June 2 and reached float altitude of 39.5 km at about 03:25 UT. Science observations ended with sunrise on the package at 11:10 UT. During the flight, we observed Jupiter to calibrate the instrument and map the telescope beam, scanned M31 (which will be reported in a future Letter), and integrated for 3.5 hr on the same CMBR field observed during the 1992 flight.

The CMBR observations were made as described in Paper I. The telescope observes near the meridian 8° above the north celestial pole and scans in azimuth ±45′ with a period of 1 minute. The scan is initially centered on a point 21′ to the east of the meridian. We track to keep this point centered in our scan until it is 21′ to the west of the meridian, then jog 42′ to the east. Each scan takes about 20 minutes, and half of each scan overlaps the preceding scan. We completed 4.5 such scans from 05:12 to 06:38 UT (called section 1 of the data) and an additional 7 scans from 07:22 to 09:43 UT (section 2). The observed field is two strips at declination $81^\circ.8 \pm 0^\circ.1$, from right ascension $15^h.27$ to $16^h.84$, and from $17^h.57$ to $19^h.71$ (all coordinates J1994.5). During the CMBR observations, the path of the balloon varied between $31^\circ.6$ and $31^\circ.9$ north latitude; thus the elevation of the telescope only varied by $0^\circ.3$ peak to peak. Figure 1 shows the fields observed in the 1992 and 1994 flights. The overlap between the fields is better than $\frac{1}{2}$ beamwidth throughout the flight. Our ability to observe exactly the same position on the sky is currently limited by the error in determining the position of the IR beam center during the initial in-flight calibration, i.e., our real-time determination of pointing is not as accurate as our postflight determination.

4. DATA ANALYSIS

4.1. *Pointing*

We determined the pointing by matching star camera images against a star catalog. This fixes the position of the camera frame at the time the exposure was taken. Between exposures, position is interpolated with the gyroscope outputs plus a small linear correction to make the gyroscope readings consistent with the camera fixes. This correction is typically 2′ in 20 minutes. The relative orientation of the camera frame and the IR telescope beam is fixed by a simultaneous observation of Jupiter with the camera and the IR telescope. The resulting absolute pointing is accurate to 2′.5 maximum error, limited by the uncertainty in the gyroscope drift correction. The pointing analysis was done in an identical way for the 1992 flight and has similar accuracy.

4.2. *Detector Data Reduction*

The instrument is calibrated by in-flight observations of Jupiter. The brightness temperatures of Jupiter for our four spectral channels are 172, 170, 148, and 148 K, derived from the spectrum of Jupiter observed by Griffin et al. (1986). The apparent diameter of Jupiter during the flight is 42″. The uncertainty in the absolute calibration is 10%, dominated by uncertainty in the referenced measurement of the brightness of Jupiter. The relative calibration uncertainty between the 1992 and 1994 flights is 5%, due to noise in the observations of Jupiter.

The detector signal contains spikes, at a rate of 0.25–0.5 s^{-1}, consistent with the hypothesis that they are due to cosmic rays striking the detectors (Charakhch'yan et al. 1978), and with the rate reported in Paper I. Cosmic rays deliver an unresolved energy impulse to the detector; we remove them by fitting the data to the impulse response function of the detector/amplifier/filter chain. We give here our results for the 5.6 cm^{-1} channel; the numbers for the other channels are similar. Candidate spike locations are identified using a 1.5 σ threshold. The data within 1 s (five detector time constants) are fitted to a model of the response function. About 2% of the spikes require a second spike near the first to be added to the fit. If the resulting spike amplitude has less than 3 σ significance, the data are left as is. If the fit is good, and the spike amplitude has more than 3 σ significance, the spike template is subtracted. A total of 5065 spikes are subtracted out of 504,000 time samples. (We allow either positive or negative amplitudes; 90% of the spikes have positive amplitude.) If the fit is poor, and the spike amplitude is significant, full data records (2 s) before and after the spike are deleted; 317 spikes were eliminated this way, removing a total of about 6% of the data.

The data are contaminated with slow drifts. The drifts are significantly correlated to air pressure, and to the pitch and roll angles of the gondola outer frame, in at least two channels. A model based on these physical parameters accounts for all but the slowest component of the drift; this is then modeled as a cubic spline with knots every 12 minutes. (This modeling was not successful for the 16.5 cm^{-1} channel, where we used a 2.5 minute knot spacing.)

We divide the sky into bins that are small compared with the beam size. The bins are $0^h.057$ in right ascension and $0^\circ.12$ in declination. Due to sky rotation, the data also need to be divided by angular orientation of the beam throw on the sky; the bin size for this coordinate is 10°. The data are then fitted to a signal in each sky bin plus the drift model. The simultaneous fit of long-term drift and sky signal ensures that this fit does not bias our observations of the sky. This fit is done separately on each channel and section of the flight. We first perform these fits without any weighting of the raw time series data; the residuals from these preliminary fits are used to estimate the instrument noise. This estimate is made by measuring the variance in the demodulated residual for each 20 minute segment of data and then propagated through the remaining processing. All χ^2 reported below are with respect to this error estimate.

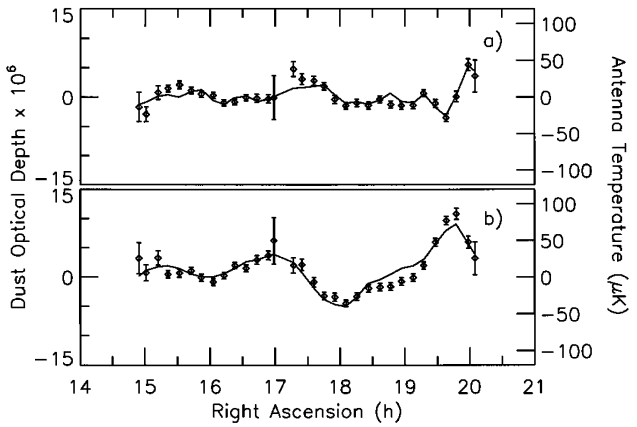

FIG. 2.—Dust optical depth times 10^6 at 22.5 cm^{-1}. The line is the brightness expected from *IRAS* 100 μm data, with the magnitude scaled to fit our observations. Scale at right is dust antenna temperature at 22.5 cm^{-1}. (*a*) Double difference; (*b*) single difference.

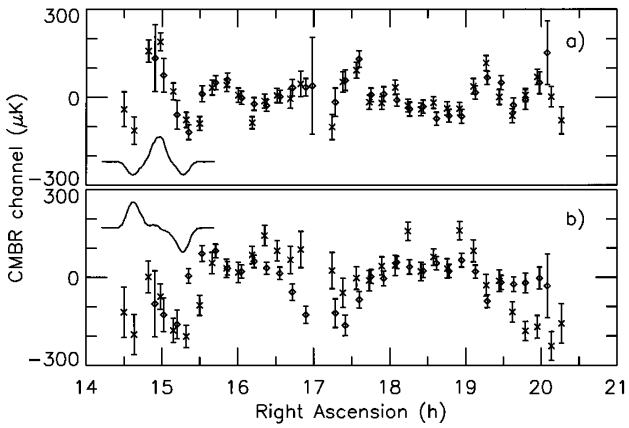

FIG. 3.—Measured CMBR anisotropy. Points with diamonds are 1994 flight; crosses are 1992 flight. The telescope beam is superposed. (*a*) Double difference; (*b*) single difference.

The fits to the sky bins plus drifts are then repeated, weighting the data with the noise estimates obtained from the first iteration. The resulting sky signals have bin-to-bin correlation, and we propagate a full covariance matrix through the remainder of the analysis. Sky bins containing less than 4 s of integration are deleted.

The data are demodulated in two different ways. The double-difference demodulation corresponds to summing the periods when the secondary is in the central position and subtracting the periods when it is to either side. This demodulation is least sensitive to atmospheric gradients and gondola swinging. The single-difference demodulation is formed by subtracting the period when the secondary is to the right from that when it is to the left, and ignoring the periods when the secondary is in the center. We use the scan over Jupiter to deduce optimal demodulations of the IR signal.

The binned data set contains 90% of all the data originally taken, with an achieved sensitivity in each of the four channels of 240, 150, 80, and 230 $\mu K\ s^{1/2}$ Rayleigh-Jeans (RJ). For channels 1 and 2 this is 490 and 850 $\mu K\ s^{1/2}$ CMBR. The offsets in the demodulated data for the different channels and demodulations range from 1 to 6 mK RJ, smaller than those reported in Paper I.

4.3. *Spectral Decomposition*

At each sky bin, we fitted the four spectral channels to a model consisting of CMBR anisotropy plus emission from warm Galactic dust. The results are not very sensitive to the parameters of the dust model; we use a dust temperature of 20 K and an emissivity index of 1.5 (consistent with Wright et al. 1991). The fit is done separately for the single- and double-difference demodulations. The χ^2/degrees of freedom (dof) for the fit is 408/430 (double difference) and 448/430 (single difference).

Figure 2 shows the resulting fitted dust optical depth at 22.5 cm^{-1}. For clarity this figure has been binned more coarsely and does not distinguish between points at slightly different declination or chop orientation; our analyses, however, do not ignore these details. We have fitted our observations to the *IRAS* Sky Survey Atlas at 100 μm (Wheelock et al. 1994) convolved with our beam patterns, with amplitude and offset as free parameters. The resulting fit is superposed on Figure 2.

The χ^2/dof of this fit is 262/210 for the double-difference demodulation and 310/210 for the single difference. The ratio of optical depths between *IRAS* and our data is consistent with an average dust emissivity spectral index between our bands and 100 μm of $\alpha = 1.40 \pm 0.16$ (still assuming a dust temperature of 20 K).

Our measurements of CMBR anisotropy are plotted in Figure 3. The measurements from 1992 are superposed. As noted earlier, there is nonnegligible correlation between the error bars on different sky bins. In making Figure 3, we have fitted out the two largest eigenmodes of the covariance matrix and used error bars formed from the diagonal of the covariance matrix after removing the two largest eigenmodes; the result is that the error bars shown in the figure can be approximately treated as uncorrelated. (This procedure is similar to that used in Fixsen et al. 1994 for the *COBE*/FIRAS calibration.) The data have also been more coarsely binned, as in Figure 2. We stress that these steps are taken only for producing representative figures; in all quantitative analyses we use the full data set and the full covariance matrix. We are in the process of calculating the correlation for the MSAM1-92 data; the 1992 data plotted here are identical to those in Paper I.

4.4. *CMBR Anisotropy*

To set limits on anisotropy in the CMBR, we assume Gaussian fluctuations with a Gaussian-shaped correlation function. We set 95% confidence level upper and lower bounds on the total rms fluctuation over the sky ($C_0^{1/2}$), assuming this correlation function with a given correlation angle θ_c. The method used is described in Paper I, although we now use a full covariance matrix for the instrument noise on the observations. The upper and lower bounds from these observations for the single- and double-difference demodulations are shown in Figure 4. The bounds for the correlation angles at which the two demodulations are most sensitive are summarized in Table 1, which also shows results for the two sections of the flight separately. The confidence intervals for both demodulations are consistent with those in Paper I.

5. CONCLUSIONS

We observed the same field in our 1992 and 1994 flights in order to determine whether the detected signal was due to

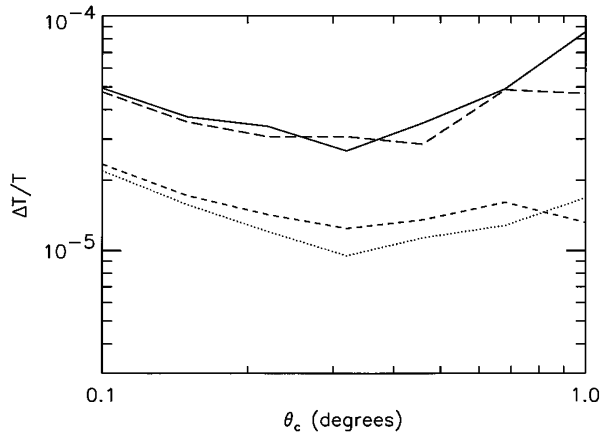

FIG. 4.—Upper and lower limits on total rms $\Delta T/T$ as a function of correlation length for Gaussian-shaped correlation functions. Plotted are 95% confidence level upper limits for the double difference (*solid line*) and single difference (*long-dashed line*), and 95% lower limits for the double difference (*dashed line*) and single difference (*dotted line*).

sidelobe pickup, atmospheric noise, or other systematic effects, or was in fact present in the sky. While we are still in the process of completing a detailed quantitative comparison of the two data sets, it is apparent that the double-difference CMBR anisotropy features reproduce quite well. This encourages us to believe that the signal we see in the double difference is present on the sky, and that contamination from atmosphere or sidelobes is small compared with the sky signal. The single-difference CMBR signal does not appear to reproduce as well. Pending completion of the more thorough comparison, we cannot rule out contamination in the single-difference channel.

TABLE 1

UPPER AND LOWER BOUNDS ON TOTAL ROOT MEAN SQUARE CMBR ANISOTROPY ($C_0^{1/2}$)

θ_c	Flight	Section	R.A.	Upper Bound (μK)	Lower Bound (μK)
			Single Difference		
0°.5.....	MSAM1-94	1	$15^h.27$–$16^h.84$	163	40
		2	17.57–19.71	75	17
		All	15.27–19.71	79	30
	MSAM1-92	All	14.44–20.33	116	53
			Double Difference		
0°.3.....	MSAM1-94	1	$15^h.27$–$16^h.84$	132	44
		2	17.57–19.71	74	24
		All	15.27–19.71	78	34
	MSAM1-92	All	14.44–20.33	97	50

NOTE.—The limits in this table do not include the calibration uncertainty.

In Paper I we pointed out that the anisotropy we observe could be due to diffuse Galactic bremsstrahlung. Recent measurements of Hα near the north celestial pole by Gaustad et al. (1995) suggest that fluctuations in bremsstrahlung from 0°.1 to 10° have a total rms of about 0.2 μK CMBR at 5.6 cm^{-1}, more than 2 orders of magnitude below the signal we report. This issue will also be addressed by our MSAM2 experiment, which will observe the same fields in five bands over 65–170 GHz.

In Paper I we also raised the possibility that the "sources" at R.A. 19^h and 15^h were either foreground sources of a previously unknown population or non-Gaussian CMBR fluctuations. This speculation was prompted by our belief that such features were inconsistent with Gaussian statistics. More careful analysis by us, and independently by Kogut, Hinshaw, & Bennett (1995), has indicated that features like these are in fact consistent with a variety of plausible correlation functions. Observations by Church et al. (1995) at 4.7 cm^{-1} rule out the source MSAM 15+82 being more compact than 2′. Therefore, removal of these regions in studies of CMBR anisotropy, as we recommended in Paper I, are a biased edit of the data, and we no longer recommend it.

Our current conclusion is that the double-difference, whole flight numbers in Table 1 are a reliable estimate of CMBR anisotropy in the observed regions. When we include the 10% uncertainty in the calibration, the resulting limits are $\Delta T/T = 1.9^{+1.3}_{-0.7} \times 10^{-5}$ (90% confidence interval) for total rms fluctuations. In the band power estimator of Bond (1995), this is $\langle \mathcal{C}_l \rangle_B = 2.1^{+1.5}_{-0.9} \times 10^{-10}$ (1 σ limits), with $\langle l \rangle = 263$.

The CMBR anisotropy channel, Galactic dust channel, pointing, covariance matrices, and beam maps are publicly available. For more information, read ftp://cobi.gsfc.nasa. gov/pub/data/msam-jun94/README.tex.

We would like to thank the staff of the National Scientific Balloon Facility (NSBF), who remain our willing partners in taking the calculated risks that result in extremely successful flights. W. Folz and J. Jewell traveled with us to the NSBF to help with flight preparations. T. Chen assisted in building and testing our new star camera system. We are grateful to M. Devlin and S. Tanaka for providing cappuccino at the crucial moment in Palestine. The Free Software Foundation provided the cross-development system for one of the flight computers. This research was supported by the NASA Office of Space Science, Astrophysics Division.

REFERENCES

Bond, J. R. 1995, Astrophys. Lett. Commun., 32, 63
Charakhch'yan, A. N., Bazilevskaya, G. A., Stozhkov, Y. I., & Charakhch'yan, T. N. 1978, in Cosmic Rays in the Stratosphere and in Near Space (Proc. P. N. Lebedev Physics Inst., Vol. 88) (New York: Consultants Bureau), 1
Cheng, E. S., et al. 1994, ApJ, 422, L37 (Paper I)
Church, S. E., Mauskopf, P. D., Ade, P. A. R., Devlin, M. J., Holzappel, W. L., Wilbanks, T. M., & Lange, A. E. 1995, ApJ, 440, L33
Clapp, A. C., et al. 1994, ApJ, 433, L57
de Bernardis, P., et al. 1994, ApJ, 422, L33
Devlin, M. J., et al. 1994, ApJ, 430, L1
Dragovan, M., Ruhl, J. E., Novak, G., Platt, S. R., Crone, B., Pernic, R., & Peterson, J. B. 1994, ApJ, 427, L67
Fixsen, D. J., et al. 1994, ApJ, 420, 457
Gaustad, J. E., Oh, E. S., McCullough, P. M., & van Buren, D. 1995, BAAS, 27, 823
Griffin, M. J., Ade, P. A. R., Orton, G. S., Robson, E. I., Gear, W. K., Nolt, I. G., & Radostitz, J. V. 1986, Icarus, 65, 244
Gundersen, J. O., et al. 1995, ApJ, 443, L57
Kogut, A., Hinshaw, G., & Bennett, C. L. 1995, ApJ, 441, L5
Netterfield, C. B., Jarosik, N., Page, L., Wilkinson, D., & Wollack, E. 1995, ApJ, 445, L69
Wheelock, S. L., et al. 1994, *IRAS* Sky Survey Atlas Explanatory Supplement (Publ. 94-11; Pasadena: JPL)
White, M., Scott, D., & Silk, J. 1994, ARA&A, 32, 319
Wilkinson, D. T. 1995, in Proc. Ninth Lake Louise Winter Inst., Particle Physics and Cosmology, ed. A. Astbury et al. (Singapore: World Scientific), 110
Wright, E. L., et al. 1991, ApJ, 381, 200